

Biomedical Physics & Engineering Express



PAPER

A study of the permeation and water-structuring behavioural properties of PEG modified hydrated silk fibroin membranes

OPEN ACCESS

RECEIVED

23 February 2021

REVISED

27 April 2021

ACCEPTED FOR PUBLICATION

30 April 2021

PUBLISHED

11 May 2021

Original content from this work may be used under the terms of the [Creative Commons Attribution 4.0 licence](#).

Any further distribution of this work must maintain attribution to the author(s) and the title of the work, journal citation and DOI.



Aisling Mann¹ , Fiona Lydon¹, Brian J Tighe¹, Shuko Suzuki² and Traian V Chirila^{2,3,4,5,6}

¹ Biomaterials Research Unit, Chemical Engineering and Applied Chemistry, College of Engineering and Physical Sciences, Aston University, Birmingham, B4 7ET, United Kingdom

² Queensland Eye Institute, South Brisbane, Queensland 4101, Australia

³ Science & Engineering Faculty, Queensland University of Technology, Brisbane, Queensland 4001, Australia

⁴ Faculty of Medicine, University of Queensland, Herston, Queensland 4029, Australia

⁵ Australian Institute for Bioengineering and Nanotechnology, University of Queensland, St Lucia, Queensland 4072, Australia

⁶ Faculty of Science, University of Western Australia, Crawley, Western Australia 6009, Australia

E-mail: a.m.mann@aston.ac.uk

Keywords: silk fibroin, poly(ethylene glycol), horseradish peroxidase, membrane permeability, water structuring

Abstract

The potential of naturally occurring substances as a source of biomedical materials is well-recognised and is being increasingly exploited. Silk fibroin membranes derived from *Bombyx mori* silk cocoons exemplify this, for example as substrata for the growth of ocular cells with the aim of generating biomaterial-cell constructs for tissue engineering. This study investigated the transport properties of selected silk fibroin membranes under conditions that allowed equilibrium hydration of the membranes to be maintained. The behaviour of natural fibroin membranes was compared with fibroin membranes that have been chemically modified with poly(ethylene glycol). The permeation of the smaller hydrated sodium ion was higher than that of the hydrated calcium ion for all three ethanol treated membranes investigated. The PEG and HRP-modified C membrane, which had the highest water content at $59.6 \pm 1.5\%$ exhibited the highest permeation of the three membranes at $95.7 \pm 2.8 \times 10^{-8} \text{ cm}^2 \text{ s}^{-1}$ compared with $17.9 \pm 0.9 \times 10^{-8} \text{ cm}^2 \text{ s}^{-1}$ and $8.7 \pm 1.7 \times 10^{-8} \text{ cm}^2 \text{ s}^{-1}$ for membranes A and B respectively for the NaCl permeant. Poly(ethylene glycol) was used to increase permeability while exploiting the crosslinking capabilities of horseradish peroxidase to increase the compressive strength of the membrane. Importantly, we have established that the permeation behaviour of water-soluble permeants with hydrated radii in the sub-nanometer range is analogous to that of conventional hydrogel polymers.

1. Introduction

Fibroin is the main proteinaceous constituent of silk threads made by larvae of the silk moth *Bombyx mori*, generally, to make webs or cocoons. A natural polypeptidic composite, it belongs to the group of fibrous proteins characterised by a recurrent sequence of amino acids. This leads to a chiefly homogeneous secondary structure, a property which responsible for the exceptional functional performance of the silk thread, critical for biomedical applications [1–5]. Silk fibroin membranes have been shown to possess appropriate physico-chemical properties and biocompatibility for a wide range of tissue engineering and biomedical applications including drug delivery and

use as implantable devices. Their in-eye use is of interest. Optimised formulations have yet to be established, however, for application in various segments of the eye such as cornea or retina. Membranes exploiting the use of silk fibroin derived from *Bombyx mori* are used currently as substrata for the growth of ocular cells with the aim of generating biomaterial-cell constructs of therapeutic significance [3, 6–13].

All potential biomaterials should have mechanical properties that are compatible with those of the host environment. They should also be wettable by, and compatible with, local biological fluids. Additionally, biomaterials should possess a degree of permeability. This can allow the movement of nutrients and gases and assist in the clearance of metabolic waste

products. Permeation also functions to support the dynamic distribution of fluid components including water, electrolytes and proteins at a sufficient level to maintain homeostasis. One area that exemplifies these requirements is a Bruch's membrane substitute. This barrier structure lies between the retina and the choroid; its permeability, to oxygen amongst other metabolic components, is vital for maintaining normal retinal function and subretinal space haemostasis [14]. Any biomaterial attempting to replicate its function must therefore show the same characteristics. The successful use of fibroin membranes to repair the outer retina of patients with age-related macular degeneration requires that these materials ideally be designed to mimic the semi-permeable barrier properties of a healthy Bruch's membrane—whilst also supporting the implantation of retinal cells.

Appropriate transport properties are therefore important for ophthalmic therapeutic applications of fibroin membranes; the ability of Bruch's membrane to allow the flow of nutrients and waste products between the retinal pigment epithelium and the choriocapillaris, which is critical for optimal function, is a significant example of this. Particular attention has been focused on oxygen permeability requirements [15, 16] and the study of transport properties of silk fibroin led to the realisation that standard fibroin membranes could potentially cause localised hypoxia following implantation [17]. This paper reviewed the permeability to oxygen of a range of fibroin-based materials and concluded that these membranes, regardless of preparation or measurement procedures, showed poor oxygen transport characteristics relative to the required level. An additional significant factor was revealed. The reported oxygen permeability measurements showed little consistency and an important aspect of this fact was the observation that the configuration of the equipment used was generally inappropriate for the nature of the samples studied [17].

The modification of fibroin membranes with other polymeric materials in order to improve physical and mechanical properties is well established [2]. There is, however, limited reported work on the use of structural modification to enhance the oxygen permeability of silk fibroin [18] and even less on its permeation to larger species such as ions and electrolytes, components essential for healthy cell propagation. This study investigated the permeant transport properties of selected silk fibroin membranes under conditions that allowed the equilibrium hydration of the membranes to be maintained. The aim was to use poly(ethylene glycol) (PEG) to improve the transport properties needed for enhanced cell proliferation and viability [9, 19] while also using the crosslinking capacity of horseradish peroxidase (HRP) as a means to improve the compressive strength of the membrane [20, 21]. As porogens, PEGs of different molecular mass have been used for silk fibroin, from 300 Da [9, 21, 22] to 900 kDa [7, 11]. While PEG of 300 Da

provides very small pores but satisfactory transport properties and mechanical strength, the PEGs with higher molecular masses provide larger pores but inferior mechanical properties. In this study we have chosen the lower molecular mass (PEG 300), which induces transport properties adequate for cells growth without compromising the mechanical properties.

2. Materials and methods

2.1. Materials

Bombyx mori silk cocoons with the pupae removed were supplied by Tajima Shoji Co. Ltd (Yokohama, Japan). Lyophilized powder horseradish peroxidase (HRP) Type VI (Lot#SLBL4932V), hydrogen peroxide (30%), poly(ethylene glycol) (PEG, MW 300 Da), phosphate buffered saline (PBS) tablets (cat. P4417), and Allura Red AC were all supplied by Sigma-Aldrich (St Louis, MO, USA). The Minisart®-GF pre-filters (0.7 μm) and Minisart® filters (0.2 μm) were supplied by Sartorius Stedim Biotech (Göttingen, Germany). The dialysis cassettes Slide-A-Layer® (MWCO 3.5 kDa), Pierce Biotechnology, USA, were supplied by Thermo Fisher Scientific (Waltham, MA, USA). A solution of cyclohexane (7% w/v) of Topas® polymer was supplied by Advanced Polymers, Frankfurt, Germany. NaCl and CaCl₂, were sourced from Sigma-Aldrich Ltd (Dorset, England). Deionized (DI) water with a conductivity of 18.2 M Ω ·cm (<20 $\mu\text{S cm}^{-1}$) (Purite Ltd, Oxon, UK) was used to make up 300 mM aqueous standard salt solutions.

2.2. Preparation of aqueous solutions of fibroin

Aqueous solutions of fibroin were formulated as previously described [6, 23]. Approx. 2.5 g of cut cocoon pieces (~1 cm² each) were placed in 1 l boiling solution of sodium carbonate (0.02 M) for 1 h to subtract the sericin component in the so-called 'degumming step'. The fibroin fibres were then treated in 1 l of water at 60 °C for 20 min, this was performed in triplicate, excess liquid was removed between each separate wash. The fibres were allowed to dry in a fume hood for at least 12 h. The dried fibres were then dissolved in a concentrated aqueous solution of lithium bromide (9.3 M) at 60 °C for 4 h to acquire a silk concentration close to 10% w/v. The fibroin solution was then slowly filtered using a 0.7 μm and then a 0.2 μm syringe filter in succession. The filtrate was dialysed using a dialysis cassette (3.5 kDa, Slide-A-Layer) against water, changing the water six times over three days. The resulting 3% w/v fibroin solution, with a was filtered again as described above and stored at 4 °C before being diluted with water to a 1.78% w/v concentration. This solution was then employed to produce the fibroin membranes.

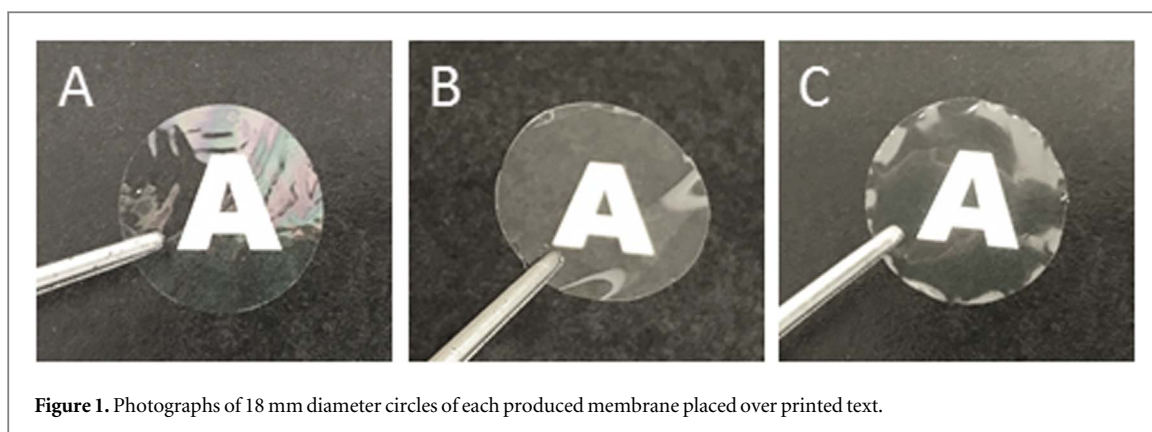


Figure 1. Photographs of 18 mm diameter circles of each produced membrane placed over printed text.

Table 1. Summary of experimental fibroin membranes.

Membrane Identity	Membrane Preparation	Cast Thickness (μm)
A	Unmodified, ethanol treated	10 ± 1
B	Unmodified, ethanol treated	30 ± 3
C	PEG ^a and HRP ^b modified, ethanol treated	30 ± 1

^a poly(ethylene glycol).

^b horseradish peroxidase.

2.3. Production of standard fibroin membranes

The standard fibroin membranes (samples A and B (table 1 and figure 1)) were cast using a custom-made casting table using 16 ml (for sample A), and 50 ml (for sample B) of the 1.78% w/v fibroin solution. The glass surface of the casting table was coated with a film obtained by evaporating 1 ml of a solution in cyclohexane (7% w/v) of Topas[®], a commercial hydrophobic olefin copolymer. The blade height was adjusted to generate approximate wet thicknesses of 10 μm and 30 μm for the resulting membranes. After drying, the membranes (while still attached to Topas[®] film) were water-annealed in a vacuum chamber at -80 kPa for six hours at RT in the presence of a vessel filled with water. Prior to further use, the Topas[®] backing film was stripped off. The final stage in A and B membrane preparation involved treatment with ethanol (immersion for 1 h, at room temperature in 70% v/v aqueous ethanol) which is a well-established method of structural consolidation [23–26].

2.4. Production of fibroin membranes mixed with low-molecular weight PEG and crosslinked with horseradish peroxidase (HRP)

The PEG-modified fibroin membranes (sample C, table 1, figure 1) were prepared according to the literature [19] with an additional step consisting of the HRP-induced crosslinking of fibroin. The enzymatic crosslinking step required HRP (150 U ml^{-1}) and H_2O_2 (0.3%) stock solutions. Separately, PEG (MW 300 Da) was gently mixed into the 1.78% fibroin solution at a PEG/fibroin ratio of 2:1 (by weight). Equal volumes of HRP and H_2O_2 solution were added to the PEG/fibroin solution and this solution was slowly stirred for a few minutes at RT. The final

concentration of HRP in the mixture was 1.1 U for 1 mg protein. For the casting step 50-mm glass Petri dishes were coated with Topas[®] polymer as described above. The PEG/fibroin/HRP solution was decanted onto the dishes and was then covered with a lid. The solution was then stored at 40 °C for two hours to form a gel. The volume was set to produce a 1.8 mg fibroin cm^{-2} approximately, to be consistent with the standard membranes. The gels were subsequently dried for 12 h at RT in a fan-driven oven. Post drying, the membranes were soaked in water for three days changing the water twice a day, to remove any residual PEG. The membranes were then treated with a 3% H_2O_2 solution for 10 min at RT to quench any unreacted HRP, they were then rinsed with water. The membranes were peeled off the Topas[®] film, treated for one hour in aqueous ethanol, and stored at 4 °C in water until use.

2.5. Fourier-transform infrared (FTIR) spectrometry

A Nicolet FTIR spectrometer (Thermo Electron Corp., USA), with a diamond attenuated total reflectance (ATR) sampling accessory, was used to characterise the formed membranes and, in particular, their secondary structure. Each spectrum was acquired by co-adding 64 scans over a range of 4000–525 cm^{-1} at a resolution of 8 cm^{-1} . Analysis and plotting of the spectra were performed with the OMNIC 7 software package (Thermo Electron Corp., USA). All membrane samples were analysed both before and after the final ethanol treatment stage.

2.6. Ion permeability: permeation cell configuration

The permeability of the silk membranes was investigated using a two cell, donor and receiver, permeation set-up (Franz Flow Cell, PermeGear Inc., Hellertown, PA, USA). 4 ml of 18.2 MΩ-cm (<20 μS cm⁻¹) deionised (DI) water was placed in the lower receiver cell (with a magnetic stirring bar). A 2 ml salt solution of either 300 mM NaCl or CaCl₂ (with a molecular weight of 58.44 and 110.98 Da respectively) was added to the upper donor cell. Individual silk membranes were sandwiched between the upper and lower chambers, sealed by two custom sized silicone O-rings. A metal clamp was used to tightly bind the upper and lower cells and each double-cell set-up was positioned on a stirring plate. A conductivity probe was placed in the side arm of the receiver chamber for continual conductivity measurement. All three ethanol treated membranes A, B and C were investigated against the two salts. In addition, all three membranes were investigated in negative control experiments, using only DI water as the permeant to assess background conductivity levels. Very low conductivity readings were observed confirming minimal background residual salt contamination with each of the membranes.

2.7. Ion permeability: conductivity measurements

A microconductivity probe (IsoPodTM, Edaq Pty. Ltd, NSW, Australia) equipped with Pod-VuTM software (Edaq Pty. Ltd, NSW, Australia), was used to measure the conductivity of the receiver solution as a function of time. The probe was interfaced through the software for automatic data collection with time. A conductivity measurement for the receiver side solution was automatically recorded at 30 s intervals for the duration of each 24-h experiment. Using calibration curves for each salt, the conductivity values were translated into millimolar concentration values enabling a concentration versus time profile to be obtained. The pH of the DI water and electrolyte solutions was not adjusted or modified and remained in the region of pH 6 during measurements.

2.8. Ion permeability: salt permeability coefficient (P)

Individual permeation coefficients (P) were calculated using equation (1):

$$P = \frac{G_t \times V_r \times h}{S \times C_d} \quad (1)$$

Where: P—permeation coefficient (cm²·s⁻¹), G_t—number of ions permeating with time (C_t/t), C_t—concentration in the receiver (mM), t—time (s), V_r - receiver volume (cm³), h - thickness of the sample (cm), S—available section for permeation (cm²), C_d—initial donor salt concentration (mM).

From the tangent to the earliest stages of the permeation profile (t < 60 min) the value of C_t/t relating to the initial concentration differential across the membrane was acquired (equation (1)). This allowed

the calculation of the permeation coefficient at a so-called P₆₀ time point as described previously [27]. The principles that underpin the conversion of experimental data to parameters that have been normalised (equation (1)) for membrane area and thickness, feed concentration and duration of experiment, have been well-established and widely exploited for over fifty years [28–32].

2.9. Effect of permeant size on membrane permeability

Membrane C, the most highly hydrated and durable membrane, was used to compare the effects of varying permeant size on permeability coefficient.

2.9.1. Allura red AC permeability

Allura Red AC (disodium 6-hydroxy-5-[(2-methoxy-5-methyl-4-sulfophenyl) azo]-2-naphthalenesulfonate) is a red dye (MW 496.42 Da) typical of those used to examine the intactness and absence of pinholes in experimental membranes. In this experiment a horizontal diffusion cell was utilised to measure the permeability coefficient for the dye. Two stirred reservoirs, one containing ~50 μg ml⁻¹ of dye in PBS (100 ml) while the other contained only PBS. The two reservoirs were separated by the fibroin membrane which was held between two customised O-rings (19-mm diameter). Aliquots (100 μl) of the PBS buffer reservoir were sampled periodically, and dye concentrations determined by absorbance at 485-nm and comparison with standard curves. Penetration rate was calculated from the slope of the concentration-time plot. The permeability coefficients were calculated from triplicate runs with equation (2), using linear initial data:

$$P = \frac{dQ}{dt} \times \frac{1}{AC_a} \quad (2)$$

Where: P is the permeability coefficient (cm s⁻¹), dQ/dt is the penetration rate of the molecule (mg s⁻¹), A is the surface area of the membrane (cm²) and C_a is the initial concentration of dye (~50 μg ml⁻¹).

2.9.2. Oxygen permeability

Oxygen permeability values were measured at a specialist service laboratory (Kureha Special Laboratory Co. Ltd, Fukushima, Japan) using an OX-TRAN Model 2/21 system (Mocon Inc., USA). This is a coulometric oxygen diffusion cell technique, typically used for much thicker contact lenses in which the sample is maintained in a humid gas stream. Oxygen permeability values (duplicate samples) for contact lens materials are conventionally expressed in Barrer units as Dk (diffusion x partition coefficient) values, where one Barrer is equivalent to 10⁻¹¹ x (cm³O₂·cm)/(cm²·s·mmHg).

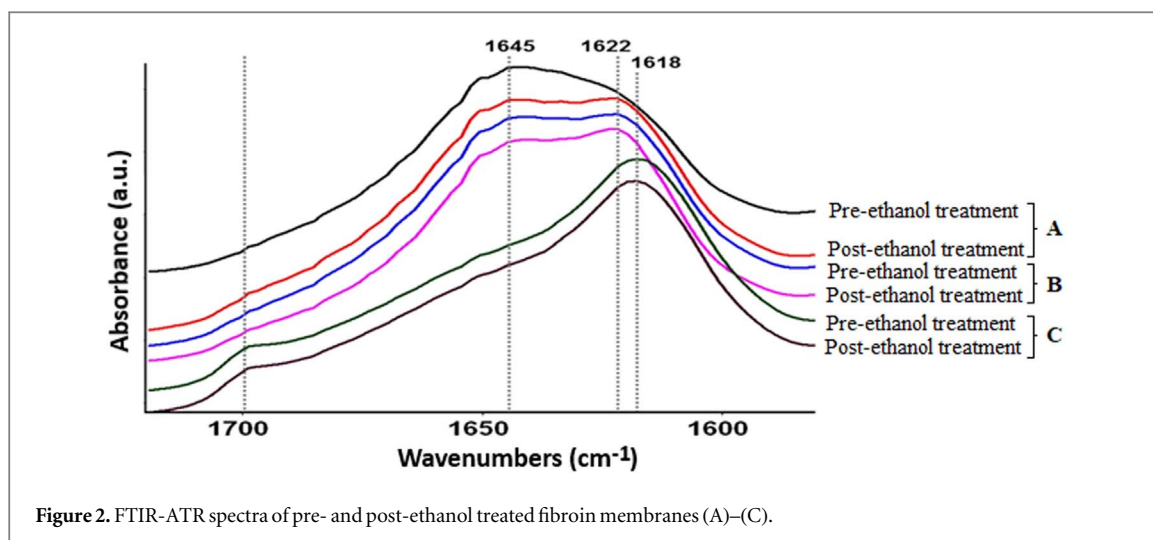


Figure 2. FTIR-ATR spectra of pre- and post-ethanol treated fibroin membranes (A)–(C).

2.9.3. Sodium ion permeability

Sodium ion permeability values were determined, as described (section 2.6), using the ion permeability Franz Flow Cell set-up.

2.10. Differential scanning calorimetry: water structuring

A differential scanning calorimeter (DSC) (DSC7, Perkin Elmer, London, UK) with a cooling system was used to obtain membrane thermograms. A piece of each membrane (cut with a size 3 cork borer) was weighed and this was then hermetically sealed in an aluminium sample pan for analysis. Each of the samples were scanned from $-50\text{ }^{\circ}\text{C}$ through to $25\text{ }^{\circ}\text{C}$ at a heating rate of $5\text{ }^{\circ}\text{C}/\text{min}$. For each individual membrane to calculate the percentage of freezing water the area measured under the melting (endotherm) peak and the heat of fusion of pure water ($79.72\text{ cal g}^{-1} = 333.55\text{ J g}^{-1}$) was used. The total area is equivalent to the total freezing water content within each membrane. When multiple peaks were observed, they were subdivided into ‘ice-like’ freezing water, this water has a melting point close to that of pure water and ‘polymer associated’ freezing water which exhibits a lower melting point. Subtraction of total freezing water from the measured equilibrium water content (EWC) calculates the non-freezing water content. The EWC was measured using a standard gravimetric technique [28, 29]. Water fractions are presented as percentages of the total weight of the hydrated membrane. Water structuring characteristics were measured after hydration in DI water and in 300 mM NaCl and 300 mM CaCl_2 salt solutions.

2.11. Statistics

Descriptive statistics in terms of mean and standard deviation (SD) are provided and relate to the variation in the individual membrane where $n \geq 3$. Correlations between membrane data are shown as p values from one-way ANOVA tests ($p < 0.05$ indicates a

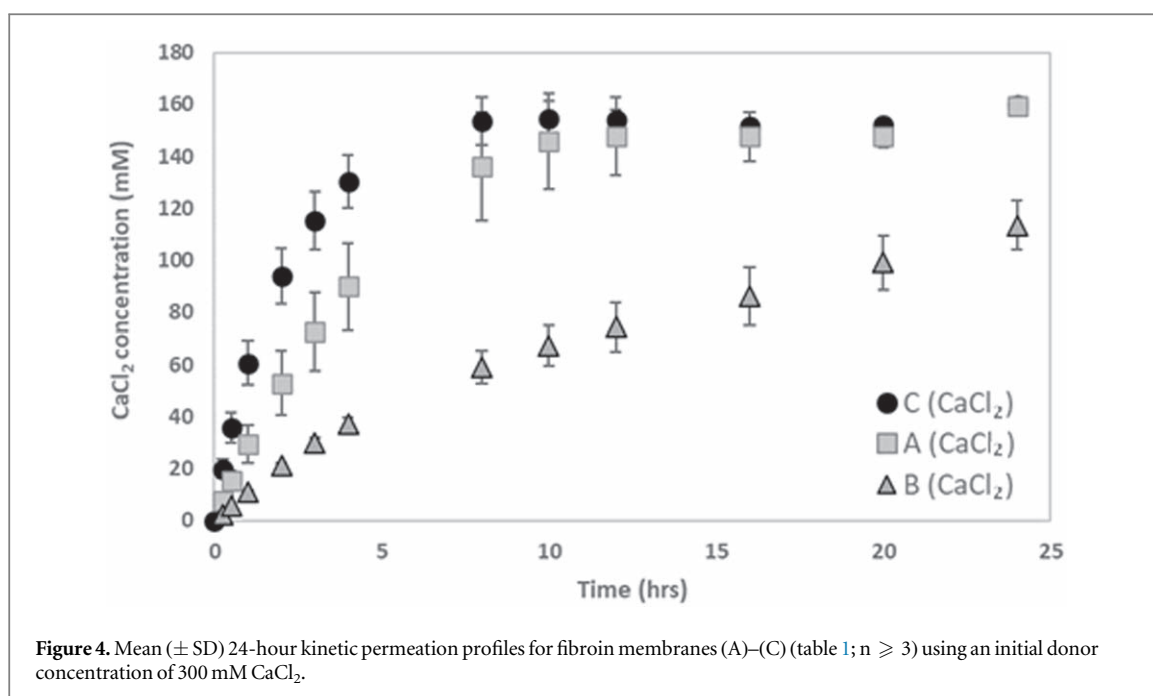
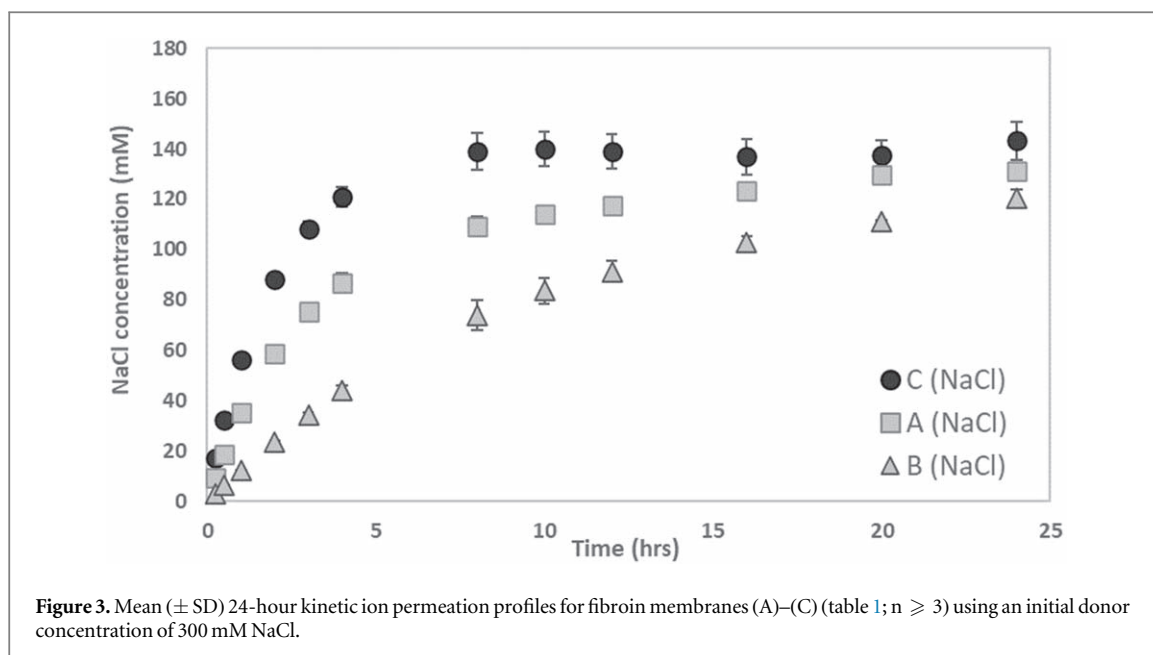
statistically significant difference), in figure 5 correlation between permeants are also provided.

3. Results

3.1. Structural analysis

The secondary structure of the silk fibroin membranes was investigated by infrared spectroscopy (figure 2), in particular the ‘amide I’ region in the FTIR-ATR spectrum ($1600\text{--}1700\text{ cm}^{-1}$) which reflects conformational transitions induced in silk fibroin during preparative stages. The Amide I region provides the most information on the secondary structure of silk fibroin, and as such the other regions are seldom employed. This absorption region is due mainly to the C=O stretching vibration in the amide groups, with a small contribution from the C–N stretching vibration, and it is commonly used for characterization of fibroin and other fibrous proteins [33–39].

As shown in figure 2, the spectrum of membrane A (before ethanol treatment) displayed a broad absorption band with two peaks at 1645 and 1622 cm^{-1} , indicating the presence of large amounts of random-coil and helical conformations respectively, and some β -sheet conformations. In the spectrum of membrane A (after ethanol treatment), the peak around 1622 cm^{-1} increased and the shoulder at 1700 cm^{-1} became more visible, indicating an enhanced content of β -sheet conformations. Samples of membrane B, which differ from A by its thickness ($30\text{ }\mu\text{m}$ instead of $10\text{ }\mu\text{m}$), already have a significant content of β -sheet conformation, and after ethanol treatment this content was slightly enhanced. The peaks corresponding to β -sheet conformations were even more significant in spectra of membrane C, with the band corresponding to random-coil (1645 cm^{-1}) being dramatically smaller than in the standard fibroin A membrane formulations. The difference between the pre- and post-ethanol treated C membrane spectra shows that



ethanol treatment had only a minimal effect of on the β -sheet content of PEG-treated fibroin membrane.

3.2. Ion permeation of fibroin membranes

Samples of the three membranes were mounted sequentially in the ion permeation cell and the permeation behaviour of sodium and calcium ions studied, in the form of their chloride salts. The primary data, in the form of ion permeation kinetic profiles are shown in figures 3 and 4 and were then converted into permeation coefficients (P_{60}) as illustrated in figure 5.

As expected, the permeation of the smaller hydrated sodium ion was higher than that of the hydrated calcium ion for all three ethanol treated membranes investigated. The PEG and HRP-modified C

membrane, which had the highest water content at $59.6 \pm 1.5\%$ (table 2) exhibited the highest permeation of the three membranes. Although membranes A and B are chemically identical, membrane A appears to show a higher permeation profile for both NaCl and particularly CaCl_2 permeation (figures 3 and 4). This is due, however, to the differences in thickness (10 versus $30 \mu\text{m}$). Figure 5 presents the permeation profiles in terms of permeation coefficient which takes thickness into account, wherein the results for membranes A and B are very similar and clearly much lower than the values exhibited by membrane C for both salt permeants (table 3). The more meaningful direct property comparisons can therefore be made between

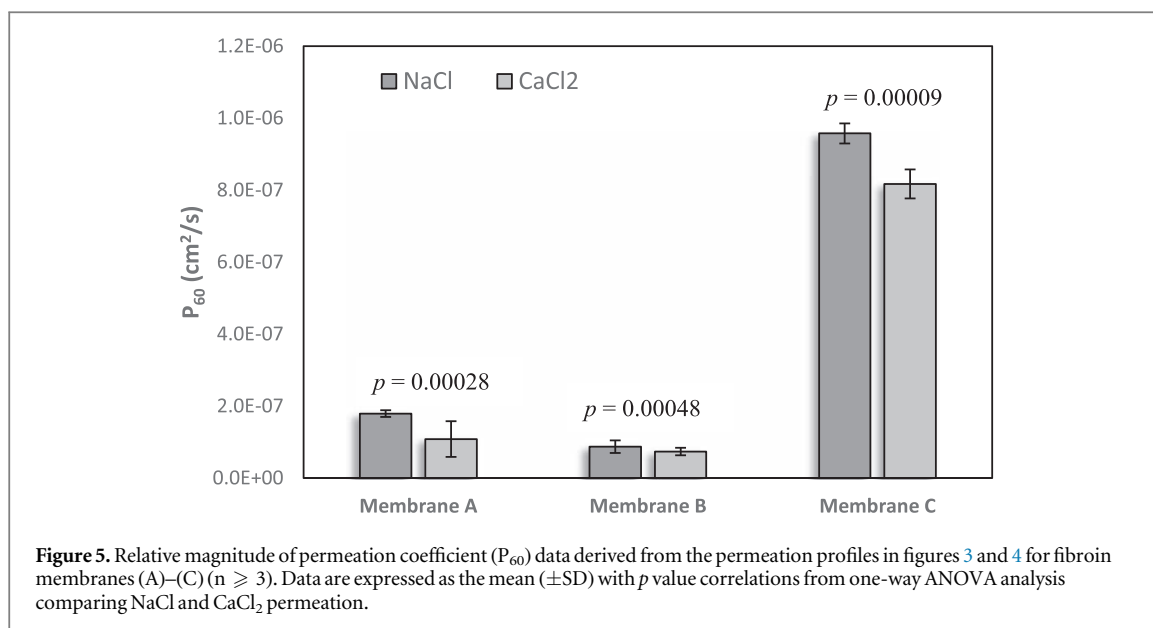


Table 2. Hydration properties of the experimental fibroin membranes A–C in DI water ($n \geq 3$). Data are expressed as the mean (\pm SD) with p value correlations from one-way ANOVA analysis comparing membranes A–C.

Membrane Identity	Equilibrium Water Content (%)	Freezing Water Content (%)	Non-freezing Water Content (%)
A	40.1 \pm 4.4	27.3 \pm 3.1	13.8 \pm 3.1
B	33.1 \pm 1.8	7.9 \pm 0.4	25.1 \pm 0.4
C	59.6 \pm 1.5	42.1 \pm 1.5	17.6 \pm 1.5
p	< 0.00001	< 0.00001	n/a

membranes B and C, which were both prepared at an equal thickness of 30 μ m.

3.3. DSC studies: water structuring

The initial studies were carried out after equilibrium hydration of the membranes in DI water. The resultant values for equilibrium water content (EWC) together with freezing and non-freezing water contents are shown in table 2. A thermogram trace for DI water on its own shows an ‘ice-like’ water peak from approximately -1°C to 3°C . It was very difficult to get reliable results for samples of membrane A, which were extremely thin (10 μ m) and fragile; it proved difficult to remove surface water robustly from samples of membrane A. This is reflected in overly high values of EWC and standard deviation, together with elevated freezing water content values. As previously stated, membrane B, which was prepared in the same way as membrane A, yields more reliable data. This applies not only to water content measurements, but also permeability values, because of the greater accuracy and consistency of thickness measurements for membrane B, relative to those for membrane A.

Because electrolytes are known to influence the structure of water, it was logical to investigate the potential effect of the permeant salts of sodium and

calcium on the water structuring of the three silk membranes. In consequence, the membranes were hydrated in 300 mM solutions of NaCl and CaCl₂—the solutions used for permeation studies. In addition to determination of EWC, total freezing water and non-freezing water, the fine structure of the melting endotherms was examined. It was clear that the behaviour of the three membranes showed significant differences. One representative DSC trace showing the water structuring profile for each of the three membranes (A–C) is provided in figure 6. The total freezing water of membranes A and B was characterised by single peaks, whereas the melting endotherm of membrane C, in all hydrating solutions showed two distinct peaks, which were readily subdivided into ‘ice-like’ water and ‘polymer associated’ water. It is logical to interpret the distinctive dual peak behaviour of membrane C as a function of the presence of the additional PEG graft chains within the hydrogel matrix. In the case of membranes A and B, where multiple peaks were not observed, the single melting point was somewhat broader and will almost certainly have some weakly polymer associated water within that main peak. The data are presented in table 3; discussion of the significance of these different aspects of behaviour in terms of the respective polymer structures is clearly important.

3.4. Membrane permeability: effect of permeant size

To obtain more information relating to the nature of the silk membranes and the permeation mechanisms involved, a wider range of permeants was examined. Membrane C being both durable and relatively highly hydrated, provided the most suitable substrate for this study. The permeants compared (presented in table 4) are oxygen gas, for which much permeation data for various classes of membrane types exists, sodium chloride, in which the hydrated sodium ion is the rate-

Table 3. NaCl and CaCl₂ permeation and DSC water structuring data in NaCl and CaCl₂ for A, B and C membranes shown in table 1. Data are expressed as the mean (\pm SD) with *p* value correlations from one-way ANOVA analysis comparing membranes A-C.

Membrane	A	B	C	<i>p</i>
NaCl P ₆₀ Permeability coefficient ($10^8 \text{ cm}^2 \text{ s}^{-1}$)	17.9 \pm 0.9	8.7 \pm 1.7	95.7 \pm 2.8	0.00001
CaCl ₂ P ₆₀ Permeability coefficient ($10^8 \text{ cm}^2 \text{ s}^{-1}$)	10.8 \pm 4.9	7.4 \pm 1.0	81.7 \pm 4.0	0.00001
Freezing Water Content in 300 mM NaCl (%)	17.1 \pm 1.6	5.7 \pm 0.4	41.9 \pm 0.6	<0.00001
of which: - Peak 1 (%) ^a	17.1 \pm 1.6	5.7 \pm 0.4	33.0 \pm 1.9	<0.00001
- Peak 2 (%) ^b	0 ^c	0 ^c	8.9 \pm 1.5	
Freezing Water Content in 300 mM Ca Cl ₂ (%)	22.1 \pm 2.9	6.3 \pm 0.6	41.2 \pm 1.3	<0.00001
of which: - Peak 1 (%)	22.1 \pm 2.9	6.3 \pm 0.6	32.5 \pm 1.2	<0.00001
- Peak 2 (%)	0 ^c	0 ^c	8.7 \pm 1.3	

^a Peak 1—‘ice-like’ freezing water.

^b Peak 2—‘polymer associated’ freezing water.

^c For membranes A and B the primary peak is broader with no distinct splitting.

determining species and Allura Red AC. Allura Red is the sodium salt of the divalent 6-hydroxy-5-[(2-methoxy-5-methyl-4-sulphophenyl)azo]-2-naphthalenesulfonate anion, which being much larger than the sodium ion is the rate determining species. Taken together, these three permeants provide a useful insight into the nature and permeation behaviour of modified silk fibroin membranes.

4. Discussion

The results presented here, and their interpretation are imparted not only in the context of the underlying structure-property relationships, but also in their relevance to the primary target application—Bruch’s membrane of the human retina. Fibroin structure is described as consisting of anti-parallel β -sheets based predominantly on a recurrent amino acid sequence of glycine and alanine with interspersed serine and tyrosine residues. The hydrogen-bond formation involving OH groups of the serine and tyrosine residues is believed to have structural implications; in addition, tyrosine has a specific functional role in these studies as a site for chemical modification of the fibroin material [42, 43].

In terms of the interpretation of the physicochemical results presented here we can regard fibroin membranes as aliphatic polyamides with different extents of modification. In some cases, as with ethanol pretreatment, there was no detectable chemical modification of the fibroin structure. The treatment is capable, however, of bringing about physical rearrangements, promoting the transition to β -sheet conformations within the fibroin polymer. These changes were detectable in the amide I region of the FTIR spectra and are exemplified in figure 2. They are reported to enhance intermolecular interactions, increase mechanical stiffness and to reduce the solubility of the

target material. As a class of materials, aliphatic polyamides show characteristically high oxygen barrier properties, to which interchain hydrogen bonding makes a major contribution. By the same token, the hydrogen bonding sites can interact with water, which occurs primarily in regions of lower crystallinity within the polymer structure. A known consequence of this interaction with water is an increase in oxygen permeability due to a deterioration in barrier properties. This is commonly recognised in the adverse effects of increased humidity on the barrier properties of polyamide films; it is a logical deduction thus that synthetic polyamide behaviour can provide the basis for the interpretation of the oxygen permeability of fibroin membranes. One important aspect of the established literature relating to the relationship between water uptake and oxygen permeability of polyamides is that no evidence has been found to support the idea that sorbed water fills fixed ‘holes’ or pores of free volume [44–46].

The assessment of the physicochemical aspects of the behavioural requirements of a Bruch’s membrane substitute has not, historically, proved to be an easy matter; ideally, a surrogate structure should mimic the physical and biochemical properties of the structure that it replaces. In terms of permeability requirements, Bruch’s membrane is a thin (3–5 μm) membrane that acts as a molecular sieve, regulating the reciprocal exchange of e.g., oxygen, electrolytes and biomolecules, including metabolic waste products that move between the retina and the general circulation. In addition, Bruch’s membrane is sufficiently permeable to allow the movement of growth factors across the membrane [47, 48]. Diffusion across the membrane is primarily regulated by passive processes and depends on its changing molecular composition, exemplified by an age-related increase in collagen cross-linking [49, 50].

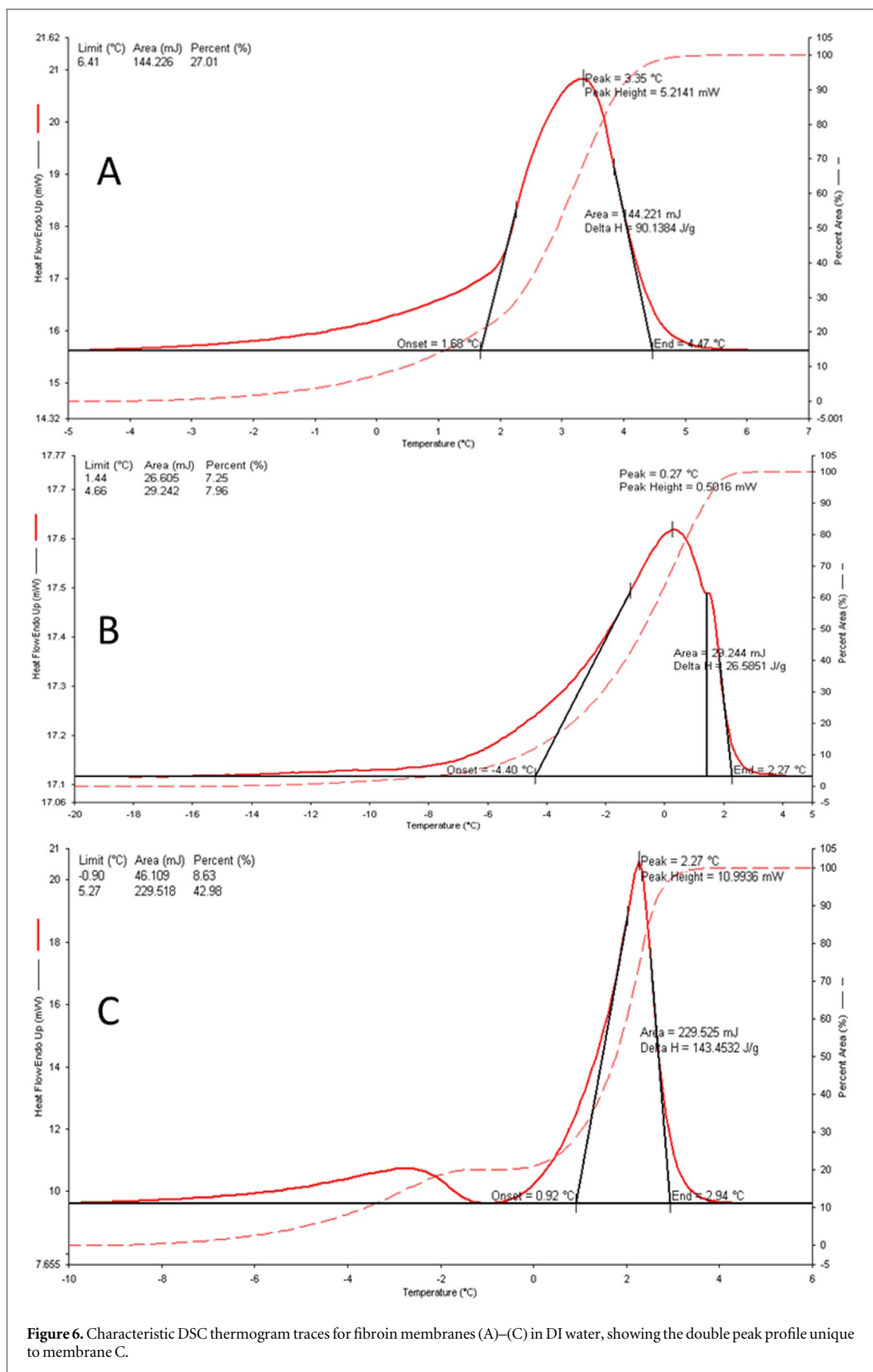


Figure 6. Characteristic DSC thermogram traces for fibroin membranes (A)–(C) in DI water, showing the double peak profile unique to membrane C.

The aim of this study was to compare and understand the behaviour of unmodified fibroin membranes with fibroin membranes that have been

chemically modified with PEG. Membranes A and B which were chemically identical but differed in thickness. Membrane A, being only 10 μm thick, was more

Table 4. Effect of permeant size on permeability coefficient of fibroin membrane C.

Permeant	Effective Diameter ^a	Permeability Coefficient ^b	Units	Permeation Cell
O ₂	ca 0.3 nm	1.98×10^{-11}	(cm ³ O ₂ ·cm)/(cm ² ·s·mmHg)	Ox-Tran (humid air)
NaCl	ca 0.7 nm	95.7×10^{-8}	cm ² ·s ⁻¹	Vertical (hydrated)
Allura Red	ca 1.6 nm	2.16×10^{-8}	cm ² ·s ⁻¹	Horizontal (hydrated)

^a Values summarised from [40, 41].

^b Values represent mean \pm 10% standard deviation.

fragile and difficult to handle. This meant that, for example, thickness and water content measurements were less reliable. The more meaningful direct property comparisons can therefore be made between membranes B and C, which were both prepared at an equal thickness of 30 μ m. However, the inclusion of membrane A was provided to show the subtle effect of thickness on some of the parameters measured here.

The structural aspects of the PEG modification process have been described wherein essentially, the combination of PEG, HRP and H₂O₂ led to the formation of more hydrophilic polymers. This can be seen by the comparative equilibrium water contents of the unmodified membrane (B, 33%) and the PEG-modified membrane (C, 60%) in table 2. The enzymatic HRP-catalysed process depends on upon the existence of 4-hydroxyphenyl side groups resulting from the presence of tyrosine in the structure. The oxidation of the tyrosine sidechain brought about by HRP and H₂O₂ is reported to result predominantly in di-tyrosine interchain linkages [20].

It is relevant to consider the possible effects of protein structure on the permeation data. The underlying question was first addressed in a comprehensive way by Scatchard [51] and subsequently by Tanford [52] who extended this theoretical basis to the use of fundamental equilibrium constant data to explain the effects of structural modification of albumin. The use of PEG modification of fibroin in the present work raises the question of PEG involvement in cation transport. This is particularly relevant to the transport of monovalent cations. The structural variations of PEG structures (for example the effects of size in both cyclic and linear structures) have been comprehensively considered [53]. In principle, these factors are of considerable relevance—particularly because cation-binding proteins are known to undergo different conformational changes and stabilisation effects with similar cations [54]. In the current study, the interaction of cations with either modified or unmodified fibroin membranes is of little practical significance. For effective ion exchange capability, the surface charge of protein domains need to carry extremely high surface charge [55] and in membrane form would need very low levels of freezing water—certainly appreciable lower than those encountered here. The membrane mass in the current studies is insignificant in comparison to the mass of permeant ions and would, in any case (because of the high levels of freezing water), be unable

to affect the transport of individual cations. Similarly, the difference in permeability coefficient between monovalent and divalent ions is entirely consistent with hydrodynamic radii and shows no dependence on structural chemistry of the membranes studied.

The nature and extent of equilibrium hydration provides information that is essential to understanding the transport mechanisms in fibroin membranes. This, in turn can explain the mechanistic role of PEG/HRP modification which has been reported to produce apparent improvements of implant behaviour in rats' cornea [19]. The hydration behaviour was conveniently assessed by examining the freezing and melting behaviour of structural water with differential scanning calorimetry. Water, that is strongly hydrogen bonded to polar groups within the polymer, does not freeze and therefore shows no melting endotherm. Water with a substantially undisturbed tetrahedral structure freezes and melts with a sharp 'ice-like' peak. More interestingly, the freezing of water can be impeded by structural interactions which reduce the perfection of the tetrahedrally-bonded ice structure with a consequent freezing point depression.

The freezing water data (tables 2 and 3) showed that changing the hydration medium from deionised water to 300 mM electrolyte solution had a small but measurable effect on the freezing water content, which is typical of the behaviour found with conventional neutral hydrogels [27]. There was a noticeable difference between the unmodified fibroin membrane (B), and the PEG-modified fibroin membrane (C) at similar thicknesses. Whereas the melting endotherm of the unmodified material showed a single 'ice-like' peak, the melting endotherm of the PEG-modified material showed two very distinct peaks—a sharp peak attributed to 'ice-like' water and broader peak of 'polymer-associated' water (figure 6). Significantly, the unmodified fibroin endotherm had a single melting peak that was observably broader than the 'ice-like' peak of the PEG-modified membrane. Just as the incorporated PEG chains exerted a significant effect on the FTIR spectrum (figure 2) they produced a marked effect on the melting endotherm. Whereas the more uniform structure of unmodified fibroin gave rise to a single peak, the presence of the secondary PEG structure within the fibroin matrix produced a very distinct secondary melting peak (figure 6(C)). The melting endotherm for membrane A was sharper than that observed with membrane B, which confirmed the previously

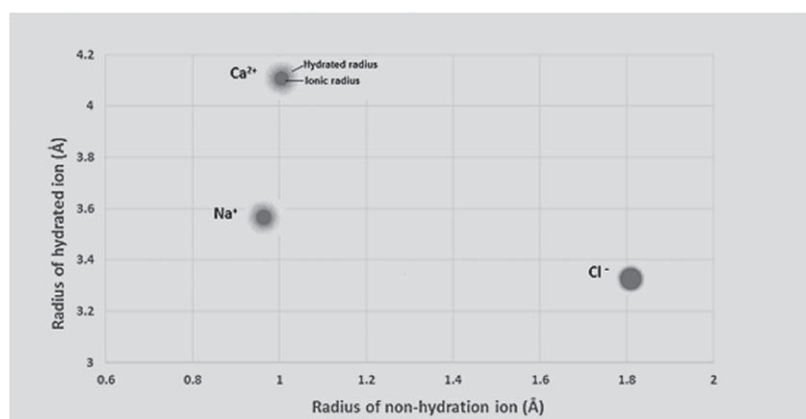


Figure 7. Schematic showing the relative ionic crystal radii in comparison to the hydrated radii for the Na⁺, Ca²⁺ and Cl⁻ ions [data extrapolated from [57]].

recorded difficulty in vigorously blotting the membrane to completely remove surface water from this much thinner and more fragile membrane.

These water structuring data provided a useful basis for understanding the ion permeation data (figure 5, table 3). There was a consistent difference between sodium ion and calcium ion permeation rates reflecting the smaller size of the hydrated sodium ion which yielded permeation rates that were generally some 10% greater than those associated with calcium permeation. The effect of water content on sodium ion permeation can most usefully be examined by comparing membranes B and C, which had the same (30 μm) thickness (table 3). Significant insight into the nature of the hydrated fibroin membranes was obtained by comparing sodium ion permeation rates with the published data for hydrogels compiled by Guan *et al* [56] which includes a graph of about fifty sodium ion permeability measurements covering water contents up to 70% made by six different groups. The fact that the results presented here for the membranes with 33% and 60% water content fit within Guan's aggregated data plot indicates that fibroin membranes show hydrogel-like permeation behaviour—which is often described as resembling dynamically fluctuating pores. As the water content increases so does the volume of water relative to that of the polymer chains. There was no evidence to support the idea that sorbed water filled holes of free volume, which is a conclusion reached in the wider studies of polyamide hydration [44, 45].

The effect of permeant size on relative permeation rates is illustrated in table 4. The Allura Red AC molecule has a molecular weight of 496.42 Da, and a sodium salt in which the sodium cation is not the species that is rate-determining in terms of permeation behaviour. This is usefully illustrated in figure 6, which shows the known relative hydrated radii in relation to the crystal radius of the ion. In the crystalline state sodium and calcium and have very similar radii but calcium has a significantly larger hydrated radius. The

figure also illustrates the fact that chloride salts are commonly used in permeation studies because the chloride anion has a hydrated radius smaller than that of sodium or potassium. In contrast, the Allura Red anion is off the scale (at 1.6 nm, 16 Å) of the y -axis of figure 7 and is clearly the rate-determining species.

In making comparisons of permeation rates involving organic solutes it was established some thirty years ago that fibroin membranes are weakly amphoteric and show pH-dependent interactions with the fibroin matrix, which can have marked effects on permeation coefficients [58]. This current study recorded fibroin water contents ranging from 30% to 32.5% at pH values between 3 and 6, consistent with the values measured here for membrane B. At pH 6 permeation coefficients varied between 0.6×10^{-7} and 1.1×10^{-7} $\text{cm}^2 \text{s}^{-1}$ for a range of neutral, anionic and cationic pharmaceuticals with molecular weights between 110 and 196 Da. Despite the complicating effects of pH and ionicity, these results are broadly consistent with those reported by Yasuda *et al* [32], for synthetic hydrogel membranes, which at a water content corresponding to the fibroin membranes and permeant molecular weights in the same range, lie between 1×10^{-7} and 2.2×10^{-7} $\text{cm}^2 \text{s}^{-1}$. The significant contribution that these two studies make to the work reported here is that all the permeation studies were carried out using permeation cells that maintain full hydration and under these conditions the permeation characteristics of fibroin membranes correspond to that of hydrogels of the same water content.

The permeation requirements for a successful Bruch's membrane substitute have not yet been clearly defined. Sodium fluorescein permeation has been used in related studies, but this was probably a function of its wider utility in ophthalmic studies [59]. Systematic studies of permeation and a comprehensive attempt to correlate literature data have suggested that size cut-off is more important than rate of permeation in Bruch's membrane itself and consequently in

surrogate materials [60]. Similarly, in studying variations in permeation rate of different hydrophilic molecules the square of molecular radius was found to provide a reasonable basis for correlations [30]. Such an approach would certainly be consistent with the relative permeation rates of sodium chloride and Allura Red through membrane C (table 4).

The questions surrounding oxygen permeability are more complex—both in terms of actual requirements for a Bruch's membrane substitute and oxygen permeation measurements for fibroin membranes. Chirila [17] undertook a comprehensive review of relevant literature reports, which suggest that silk fibroin membranes have a Dk value of between 1 and 10 Barrers, and the commercial laboratory measurement on membrane C reported here (table 4) is consistent with these literature findings. These various results would suggest that the various silk fibroin samples with reported oxygen permeability measurements may be far less permeable to oxygen than would be required for a surrogate Bruch's membrane. It is important that in this application fibroin must be permeable enough to allow a minimum amount of oxygen to diffuse through the sub-retinal space in order to maintain retinal function; this would clearly depend on the thickness and size of the silk fibroin implant, but the target permeability of the material should not be greatly less than that of the structure that it replaces. Although there is no experimentally established oxygen permeability for Bruch's membrane itself there has been a consistent interest in the oxygen permeability of human and animal tissue explanted from a variety of body sites, including the eye [61, 62]. Many soft tissue sites have water contents of 60% or more and oxygen permeabilities equivalent to Dk values around 30 Barrers—considerably greater than the reported permeability values of fibroin membranes.

It is a logical principle that any biomaterial property measurement should be carried out in an environment that mimics that of the target site as closely as possible. Bruch's membrane exists in an enclosed environment with no air interface. Early fundamental studies of hydrogel oxygen permeability were also carried out in stirred cells that maintained full hydration [63]. As the importance of oxygen permeability for corneal health became more widely understood and the commercial application of hydrogels as contact lenses grew, however, so did the need for convenient techniques to measure lens permeability. Similarly, with the advent of high permeability silicone hydrogels the earlier polarographic technique was supplemented with what is referred to as the coulometric technique in which a constant stream of humid carrier gas flows over the surface of the sample [64].

These techniques have been optimised for contact lens use and taking for instance edge effects and boundary layer effects into account, the results apply well to the contact lens, operating as it does at an air

interface. It must be noted that the average (centre-to-edge) thickness of the contact lens test sample will normally be of the order of 100 μm , and although the coulometric method will yield oxygen permeability results for a 30- μm fibroin sample it is to be anticipated that the combined effect of fractional water loss and boundary layer effects will lead to a marked underestimate of the true permeability of a fibroin sample maintained at its equilibrium hydration level.

Two other facts support this contention. Firstly, the Dk values of conventional hydrogels are governed by water content and the Dk values of the unmodified fibroin membrane (B) and the PEG-modified membrane (C) at equilibrium hydration would be expected to be *ca* 8 Barrers and *ca* 25 Barrers, respectively. Secondly, the ion permeation values of the fully hydrated membranes studied here show that, in terms of permeability characteristics, the hydrated fibroin membranes behave as hydrogels and would be expected to show much higher oxygen permeabilities than reported. Essentially, fibroin samples do not give sound results when used directly with techniques designed for hydrogel contact lenses.

The fact that the permeability of both unmodified and PEG-modified fibroin to hydrated ions is consistent with that of hydrogel polymers confirms that their permeability to water-soluble species, including oxygen, will follow a similar pattern. There is evidence that acceptable permeation behaviour for a Bruch's membrane substitute is related to cut-off size in addition to permeation rate. We have demonstrated effective transport behaviour up to a permeant diameter of approximately 1.5 nm with Allura Red AC experiments. Further experiments will be necessary to establish the upper cut-off limits.

5. Conclusions

Silk fibroin membranes present an obvious potential for use in ocular tissue engineering. It is essential to assess both cellular and extracellular matrix outcomes in addition to electrolytes and metabolite interaction, as this will dictate tissue-specific architectural and biomaterial design. However, the aim of this study was to establish and focus on the specific permeation behaviour of fibroin membranes under conditions that are relevant to their application such as Bruch's membrane substitutes. Explorative studies investigating cellular interactions with silk biomaterials are critical and some interesting studies have been published which offer an insight into this new and emerging field [6, 65, 66].

Of interest was the extent to which the PEG-modification protocol improved the permeability of the unmodified silk fibroin membranes. Importantly, we have established that the permeation behaviour of water-soluble permeants with hydrated radii in the sub-nanometer range is analogous to that of

conventional hydrogel polymers. In this respect it is apparent the PEG-modified fibroin has oxygen and electrolyte transport characteristics similar to those of soft tissue found in many body sites. It will be important to establish the upper size cut-off limit of the PEG-modified fibroin membrane since that is believed to be an important characteristic of the target structure and will be influenced by the combination of chemical and physical crosslinks in the modified fibroin matrix. In this respect it is unlikely that any semi-synthetic material will precisely match the target structure, which is described as an elastin- and collagen-rich extracellular matrix that acts as a molecular sieve, but the PEG-modification described here greatly enhances the potential of fibroin as a Bruch's membrane surrogate.

Data availability statement

The data that support the findings of this study are available upon reasonable request from the authors.

Disclosures

The authors declare no conflict of interest.

ORCID iDs

Aisling Mann  <https://orcid.org/0000-0002-4075-8831>

References

- [1] Vepari C and Kaplan D L 2007 Silk as a biomaterial *Prog. Polym. Sci.* **32** 991–1007
- [2] Murphy A R and Kaplan D L 2009 Biomedical applications of chemically-modified silk fibroin *J. Mater. Chem.* **19** 6443–50
- [3] Harkin D G, George K A, Madden P W, Schwab I R, Hutmacher D W and Chirila T V 2011 Silk fibroin in ocular tissue reconstruction *Biomaterials* **32** 2445–58
- [4] Kundu B, Kurland N E, Bano S, Patra C, Engel F B, Yadavalli V K and Kundu S C 2014 Silk proteins for biomedical applications: bioengineering perspectives *Prog. Polym. Sci.* **39** 251–67
- [5] Kapoor S and Kundu S C 2016 Silk protein-based hydrogels: Promising advanced materials for biomedical applications *Acta Biomater.* **31** 17–32
- [6] Chirila T V., Barnard Z., Zainuddin D G H, Schwab I.R. and Hirst L.W. 2008 Bombyx mori silk fibroin membranes as potential substrata for epithelial constructs used in the management of ocular surface disorders *Tissue Eng. A* **14** 1203–11
- [7] Lawrence B D, Marchant J K, Pindrus M A, Omenetto F G and Kaplan D L 2009 Silk film biomaterials for cornea tissue engineering *Biomaterials* **30** 1299–308
- [8] Gil E S, Mandal B B, Park S-H, Marchant J K, Omenetto F G and Kaplan D L 2010 Helicoidal multi-lamellar features of RGD-functionalized silk biomaterials for corneal tissue engineering *Biomaterials* **31** 8953–63
- [9] Higa K, Takeshima N, Moro F, Kawakita T, Kawashima M, Demura M, Shimazaki J, Asakura T, Tsubota K and Shimmura S 2011 Porous silk fibroin film as a transparent carrier for cultivated corneal epithelial sheets *J. Biomater. Sci. Polym.* **22** 2261–76
- [10] Madden P W, Lai J N X, George K A, Giovenco T, Harkin D G and Chirila T V 2011 Human corneal endothelial cell growth on a silk fibroin membrane *Biomaterials* **32** 4076–84
- [11] Shadforth A M A, George K A, Kwan A S, Chirila T V and Harkin D G 2012 The cultivation of human retinal pigment epithelial cells on Bombyx mori silk fibroin *Biomaterials* **33** 4110–7
- [12] Chirila T V, Suzuki S, Hirst L W and Harkin D G 2016 Reconstruction of the ocular surface using biomaterial templates *Biomaterials and Regenerative Medicine in Ophthalmology* ed T V Chirila and D G Harkin 2nd (Amsterdam: Woodhead Publishing Series in Biomaterials The Netherlands) 178–218 Elsevier Ltd
- [13] Shadforth A M A, Chirila T V, Harkin D G, Kwan A S L and Chen F K 2016 Biomaterial templates for the culture and transplantation of retinal pigment epithelial cells: a critical review *Biomaterials and Regenerative Medicine in Ophthalmology* ed T V Chirila and D G Harkin 2nd. (Amsterdam: Woodhead Publishing Series in Biomaterials The Netherlands) 263–89 Elsevier Ltd
- [14] Stefánsson E, Geirsdóttir Á and Sigurdson H 2011 Metabolic physiology in age related macular degeneration *Prog. Ret. Eye Res.* **30** 72–80
- [15] Wong-Riley M 2010 Energy metabolism of the visual system *Eye Brain* **2** 99–116
- [16] Country M W 2017 Retinal metabolism: a comparative look at energetics in the retina *Brain Res.* **1672** 50–7
- [17] Chirila T V 2017 Oxygen permeability of silk fibroin membranes: a critical review and personal perspective *Biomater. Tissue Technol.* **1** 1–5
- [18] Ratanasongtham P, Watanesk R and Watanesk S 2013 Comparison of porosity improvement of silk fibroin membrane using polyethylene glycol and glutaraldehyde for increasing oxygen permeability *Adv. Mater. Res.* **750–752** 1601–8
- [19] Suzuki S, Dawson R A, Chirila T V, Shadforth A M A, Hogerheyde T A S, Edwards G A and Harkin D G 2015 Treatment of silk fibroin with poly(ethylene glycol) for the enhancement of corneal epithelial cell growth *J. Funct. Biomater.* **6** 345–66
- [20] Chirila T V, Suzuki S and Papolla C 2017 A comparative investigation of Bombyx mori silk fibroin hydrogels generated by chemical and enzymatic cross-linking *Biotechnol. Appl. Biochem.* **64** 771–81
- [21] Suzuki S et al 2019 Optimization of silk fibroin membranes for retinal implantation *Mater. Sci. Eng. C* **105** 110131
- [22] Demura M and Asakura T 1991 Porous membrane of Bombyx mori silk fibroin: structure, characterization, physical properties and application to glucose oxidase immobilization *J. Membr. Sci.* **59** 39–52
- [23] Bray L J, George K A, Ainscough S L, Hutmacher D W, Chirila T V and Harkin D G 2011 Human corneal epithelial equivalents constructed on Bombyx mori silk fibroin membranes *Biomaterials* **32** 5086–91
- [24] Bray L J, George K A, Suzuki S, Chirila T V and Harkin D G 2013 Fabrication of a corneal-limbal tissue substitute using silk fibroin *Meth. Mol. Biol.* **1014** 165–78
- [25] Jeong L, Lee K Y, Liu L W and Park W H 2006 Time-resolved structural investigation of regenerated silk fibroin nanofibers treated with solvent vapor *Int. J. Biol. Macromol.* **38** 140–4
- [26] Nogueira G M, Rodas A C, Leite C A, Giles C, Higa O Z, Polakiewicz B and Beppu M M 2010 Preparation and characterization of ethanol-treated silk fibroin dense membranes for biomaterials application using waste silk fibers as raw material *Bioresour. Technol.* **101** 8446–51
- [27] Mann A, Sáez-Martínez V, Lydon F and Tighe B J 2019 Investigating the permeation properties of contact lenses and its influence on tear electrolyte composition *J. Biomed. Mater. Res. B Appl. Biomater.* **107** 1997–2005

- [28] Hamilton C J, Murphy S M, Atherton N D and Tighe B J 1998 Synthetic hydrogels: 4, The permeability of poly(2-hydroxyethyl methacrylate) to cations - an overview of solute-water interactions and transport processes *Polymer* **29** 1879–86
- [29] Murphy S M, Hamilton C J and Tighe B J 1998 Synthetic hydrogels: 5, Transport processes in 2-hydroxyethyl methacrylate copolymers *Polymer* **29** 1887–93
- [30] Kim S W, Cardinal J R, Wisniewski S and Zentner G M 1980 Solute permeation through hydrogel membranes: hydrophilic versus hydrophobic solutes *Water in Polymers*, ed S P Rowland 127, (DC: American Chemical Society Washington) p 347–59 ACS Symp. Ser.
- [31] Yasuda H, Lamaze C E and Ikenberry L D 1968 Permeability of solutes through hydrated polymer membranes. Part I. Diffusion of sodium chloride *Makromol. Chem.* **118** 19–35
- [32] Yasuda H, Ikenberry L D and Lamaze C E 1969 Permeability of solutes through hydrated polymer membranes. Part II. Permeability of water soluble organic solutes *Makromol. Chem.* **125** 108–18
- [33] Ambrose E J and Elliot A 1951 Infra-red spectra and structure of fibrous proteins *Proc. Roy. Soc. A* **206** 206–19
- [34] Ambrose E J, Bamford C H, Elliot A and Hanby W E 1951 Water-soluble silk: an α -protein *Nature* **167** 264–5
- [35] Lenormant H 1956 Infra-red spectra and structure of the proteins of the silk gland *Trans. Faraday Soc.* **52** 549–53
- [36] Yoshimizu H and Asakura T 1990 The structure of Bombyx mori silk fibroin membrane swollen by water studied with ESR, ¹³C-NMR, and FT-IR spectroscopies *J. Appl. Polym. Sci.* **40** 1745–56
- [37] Jackson M and Mantsch H H 1995 The use and misuse of FTIR spectroscopy in the determination of protein structure *Crit. Rev. Biochem. Mol. Biol.* **30** 95–120
- [38] Wilson D, Valluzzi R and Kaplan D 2000 Conformational transitions in model silk peptides *Biophys. J.* **78** 2690–701
- [39] Chen X, Knight D P, Shao Z and Vollrath F 2001 Regenerated Bombyx mori silk solutions studied with rheometry and FTIR *Polymer* **42** 9969–74
- [40] O'Hern S C, Boutlier M S H, Idrobo J-C, Song Y, Kong J, Laoui T, Atieh M and Karnik R 2014 Selective ionic transport through tunable subnanometer pores in single-layer graphene membranes *Nano Lett.* **14** 1234–41
- [41] O'Hern S C 2015 Nanoporous monolayer graphene membranes for water purification: From concept to realization *PhD Thesis* Massachusetts Institute of Technology, USA Department of Mechanical Engineering <https://dspace.mit.edu/handle/1721.1/97841>
- [42] Asakura T, Suita K, Kameda T, Afonin S and Ulrich A S 2004 Structural role of tyrosine in Bombyx mori silk fibroin, studied by solid-state NMR and molecular mechanics on a model peptide prepared as silk I and II *Magn. Reson. Chem.* **42** 258–66
- [43] Asakura T, Ohgo K, Ishida T, Taddei P, Monti P and Kishore R 2005 Possible implications of serine and tyrosine residues and intermolecular interactions on the appearance of silk I structure of Bombyx mori silk fibroin-derived synthetic peptides: high resolution C-13 cross-polarization/magic-angle spinning NMR study *Biomacromolecules* **6** 468–74
- [44] Litvinov V M, Persyn O, Miri V and Lefebvre J M 2010 Morphology, phase composition, and molecular mobility in polyamide films in relation to oxygen permeability *Macromolecules* **43** 7668–79
- [45] Hu Y S, Mehta S, Schiraldi D A, Hiltner A and Baer E 2005 Effect of water sorption on oxygen-barrier properties of aromatic polyamides *J. Polym. Sci., Part B: Polym. Phys.* **43** 1365–81
- [46] Murthy N S 2006 Hydrogen bonding, mobility, and structural transitions in aliphatic polyamides *J. Polym. Sci., Part B: Polym. Phys.* **44** 1763–82
- [47] Bok D 1993 The retinal pigment epithelium: a versatile partner in vision *J. Cell Sci. Suppl.* **17** 189–95
- [48] Booi J C, Baas D C, Beisekeeva J, Gorgels T G M F and Bergen A A B 2009 The dynamic nature of Bruch's membrane *Prog. Ret. Eye Res.* **29** 1–18
- [49] Hewitt A T, Nakazawa K and Newsome D A 1989 Analysis of newly synthesized Bruch's membrane proteoglycans *Invest. Ophthalmol. Vis. Sci.* **30** 478–86
- [50] Galloway C A et al Characterization of human iPSC-RPE on a prosthetic Bruch's membrane manufactured from silk fibroin *Invest. Ophthalmol. Vis. Sci.* **59** 2018 2792–800
- [51] Scatchard G 1949 The attractions of proteins for small molecules and ions *Annals NY Acad. Sci.* **51** 660–72
- [52] Tanford C 1950 Preparation and properties of serum and plasma proteins. XXIII. hydrogen ion equilibria in native and modified human serum albumins *J. Am. Chem. Soc.* **72** 441–451
- [53] Poudel L, Podgornik R and Ching W-Y 2017 The hydration effect and selectivity of alkali metal ions on poly(ethylene glycol) models in cyclic and linear topology *J. Phys. Chem. A* **121** 4721–31
- [54] Arias-Moreno X, Abian O, Vega S, Sancho J and Velazquez-Campoy A 2011 Protein-cation interactions: structural and thermodynamic aspects *Curr. Protein Pept. Sci.* **12** 325–38
- [55] Gräslund T, Lundin G, Uhlén M, Nygren P-Å and Hober S 2000 Charge engineering of a protein domain to allow efficient ion-exchange recovery *Prot. Eng. Design Selection.* **13** 703–9
- [56] Guan L, Gonzalez Jimenez M E, Walowski C, Boushehri A, Prausnitz J M and Radke C J 2011 Permeability and partition coefficient of aqueous sodium chloride in soft contact lenses *J. Appl. Polym. Sci.* **122** 1457–71
- [57] Nightingale E R Jr 1959 Phenomenological theory of ion solvation. effective radii of hydrated ions *J. Phys. Chem.* **63** 1381–7
- [58] Chen J, Minoura N and Tanioka A 1994 Transport of pharmaceuticals through silk fibroin membrane *Polymer* **35** 2853–6
- [59] Moldow B, Larsen M, Sander B and Lund-Andersen H 2001 Passive permeability and outward active transport of fluorescein across the blood-retinal barrier in early ARM *Br. J. Ophthalmol.* **85** 592–7
- [60] Lee C J, Vroom J A, Fishman H A and Bent S F 2006 Determination of human lens capsule permeability and its feasibility as a replacement for Bruch's membrane *Biomaterials* **27** 1670–8
- [61] Freeman R and Fatt I 1972 Oxygen permeability of the limiting layers of the cornea *Biophys. J.* **12** 237–47
- [62] Weissman B A, Selzer K, Duflin R M and Perrir T H 1983 Oxygen permeability of rabbit and human corneal stroma *Invest. Ophthalmol. Vis. Sci.* **24** 645–7
- [63] Ng C O and Tighe B J 1976 Polymers in contact lens applications VI. The 'dissolved' oxygen permeability of hydrogels and the design of materials for use in continuous-wear lenses *Br. Polym. J.* **8** 118–23
- [64] Fatt I 1989 Comparison of the single-chamber polarographic and the coulometric carrier gas procedures for measuring oxygen permeability *Int. Contact Lens Clinic* **16** 226–31
- [65] Lawrence B D, Marchant J K, Pindrus M A, Omenetto F G and Kaplan D L 2009 Silk film biomaterials for cornea tissue engineering *Biomaterials* **30** 1299 e308
- [66] Gil E S, Park S H, Marchant J, Omenetto F and Kaplan. D L 2010 Response of human corneal fibroblasts on silk film surface patterns *Macromol. Biosci.* **10** 664 e73